International Journal of Engineering

Static Coil Design Considerations for the Magnetic Resonance Imaging

M. Shiravi*[a], B. Ganji[a], A. Shiravi[b]

[a] Department of Electrical & Computer Engineering, University of Kashan, Kashan, Iran
[b] Department of Radiology, Faculty of Medicine, Tehran University of Medical Sciences, Tehran, Iran

P A P E R   I N F O

A B S T R A C T

One of the main challenges in developing magnetic resonance imaging (MRI) systems is to create a static coil that needs to generate magnetic field density along with the characteristics of optimal homogeneity and magnitude size. To do this, two N42 Block PMs are used and the iron core is designed and optimized in accordance with the dimensions of PM pieces using ANSYS Maxwell software. Then, all iron parts are lathed, the yoke pieces and pole spacers are welded. In addition, PM and pole pieces are installed. Finally, measurement is done by Lutron to evaluate the static coil performance.

1. INTRODUCTION

One of the most important medical diagnostic imaging modality is MRI. In addition, how to assemble the configuration of the magnet is so important and it affects the quality of the MRI. Two main types of magnets which are recently used in the MRI are permanent and superconducting magnets. Due to high intensity, superconducting magnets become more popular but they are so expensive and special equipments are needed for cooling. In comparison to superconducting magnets, permanent magnets produce a smaller intensity but they consume less electricity. In addition, they do not need to the cooling equipments and therefore its construction cost is lower. Recently, permanent magnet assemblies have been applied to the manufacturing of the MRI for different applications. How to use the permanent magnets and their shape can affect the quality of imaging. Using some extra pole pieces of iron, the uniformity of the magnetic field can be also improved [1].

In a permanent MRI system, shimming rings are commonly used to improve field homogeneity. To design a small permanent magnet system, the application of sensitivity analysis and particle swarm optimization algorithm are reported in literature [2] for the optimization of shimming rings. Taking account of the pulse excited gradient coil field, the ferromagnetic pole pieces of permanent magnet assembly for the MRI is designed in literature [3]. In this optimal design, both the transient design sensitivity analysis and the three-dimensional finite element method are used to give a search direction. The claustrophobia of a patient can be reduced using the MRI superconducting magnet with openness. To fabricate an open MRI magnet, a different magnet configuration with iron rings and pole plates balancing the force between the coil and the yoke is introduced in literature [4] to correct the field homogeneity. The homogeneity of magnetic field is one of the most critical parameter of MRI magnet. To correct the inhomogeneity of the basic filed, a passive shimming method based on magnetic coupling model and niching genetic algorithm is introduced in literature [5]. In the MRI system, gradient coils are the responsible components for encoding the volume of interest. The electromagnetic and thermal gradient coil properties are investigated in literature [6] and two cooling system are introduced to cool them.

According to this law that the different material susceptibilities affect the homogeneity of the magnetic field density (B_0), the passive shimming is performed in

*Corresponding Author Email: m.shiravi@grad.kashanu.ac.ir (M. Shiravi)

research article [7] by covering the skin using matching the magnetic susceptibility of materials. To achieve a possible pole plate structure and field uniformity for a non-axial ellipsoid structure, an optimization algorithm is designed in literature [8]. The shape of the pole piece is optimized by the finite element method, thereby creating the desired field density for imaging. Static magnet design aspects that should be considered are: strength, temporal stability, minimization of fringe, homogeneity, patient access, and cost of productivity. It is reported in literature [9], spherical harmonics are eliminated by the shimming of iron pieces. The configuration of pieces is determined by the micro genetic algorithm to make the magnetic field uniform. This means that these pieces are configured in such a way that the sum of the spherical harmonic coefficients of the magnet and iron pieces will be zero. Weggel and Weggel reported [10] have proposed, a general history of the open MRI system. Then, the dimensions and parameters related to the optimal design of 24 static coils with the uniform magnetic field are presented in the table. At the end, it should not be forgotten that there are a large number of ambiguities and challenges about the possibility of developing this system.

In the present paper, the main goal is to generate a uniform and homogenous field in the air gap. The idea is indeed finding a solution for the limitation. For this purpose, a rectangular cube (block) permanent magnet should be used which is different from this assumption that a disc type permanent magnet should be used. In this case, an optimized block pole piece ought to be utilized. The pole spacer must also be a block piece. Nevertheless, the area of interest is always considered spherical (which is the same in this study) because there is always a sphere that is inscribed in a cube. In the following, the theory and required mathematical equations are described in section 2. Iron core design aspects are introduced in section 3. The iron core construction is then presented in section 4. Finally, the paper is concluded in section 5.

2. REQUIRED MATHEMATICAL EQUATIONS

There are two types of sources for the magnetic field inhomogeneity:
First: the inhomogeneity arises from the inappropriate structure of the static coil. Generally, the z-component of magnetic field density in terms of spherical harmonics in the ROI (region of interest) in a given sphere, calculated as follows [11]:

$$B_z = \sum_{n=0}^{\infty}\sum_{m=-n}^{n}\left(\frac{r}{r_0}\right)^n P_m^n(cos\alpha)[a_{nm}\cos(m\beta) + b_{nm}\sin(m\beta)] \tag{1}$$

where $r, \alpha,$ and β are spherical coordinates, r_0 is the radius of ROI, and $P_m^n(cos\alpha)$ are Legendre polynomials,

a_{nm} and b_{nm} are homogeneity coefficients: the more homogeneity, the smaller the coefficients. In optimization process, the objective function (f) should be minimized as follows [12]:

$$f = \sqrt{\frac{1}{N}\sum_{i=1}^{N}(B_{zi} - B_0)^2} \tag{2}$$

where N is the total number of sample points, B_{zi} is the sample magnetic flux density in the ROI which strongly depends on the shape of the pole piece and the air gap length, B_0 is the homogeneity goal value at ROI centre.
Second: The heterogeneity resulting from the structure of the sample is important [7]. The field variations are achieved by the phase difference of two images obtained at two different echo times. Then, the phase difference is proportional to the frequency of nuclei process (ω) and it is produced by the changes in echo times (TE):

$$\Delta\phi = \phi_2 - \phi_1 = \omega\Delta\text{TE} = \omega(TE_2 - TE_1) \tag{3}$$

where $\phi_1 = \phi_0 + \omega TE_1, \phi_2 = \phi_0 + \omega TE_2$. ϕ_0 is the initial phase which is produced by RF coil. By substituting $\omega = \gamma\Delta B_0$ (γ is the gyromagnetic ratio of nuclei) in equation (1), field inhomogeneity is obtained:

$$\Delta B_0 = \frac{\Delta\phi}{\gamma\Delta\text{TE}} \tag{4}$$

3. IRON CORE DESIGN ASPECTS

It is obvious that magnetic field density of air gap is improved by using iron core, then finding optimal dimensions for the iron core yoke should be discussed. For example, the distance between two PM pieces (50×100 mm^2, and 25 mm thickness) is increased from 0 mm to 50 mm, and the variation of force is shown in Figure 1. When the pole pieces are used, the force is strengthened. Comparison between two modes (with pole pieces and without pole pieces) is shown in Figure 2. Similarly, the appropriate magnet distance from the yoke's walls is obtained.

Figures 3 and 4 show one-sided and two-sided cores, respectively. In Table 1, the dimensions of these configurations are shown (with thickness 25 mm for all parts). Figure 5 shows the distribution of magnetic field density through the iron core. Magnetic field density for the one-sided core is shown in Figure 6. Also, Figures 7 and 8 show for the two-side core.

3. 1. Inhomogeneity   The region of interest is assumed to be spherical with a diameter of 50 mm which is known as a certain diameter of spherical volume (DSV). Inhomogeneity in the region is defined in the following equation [13]:

$$\eta = \frac{B_{max} - B_{min}}{B_{mean}} \times 10^6 \tag{5}$$

where B_{max}, B_{min}, and B_{mean} are respectively maximum, minimum, and average of the magnetic flux density in the region. The unit of η is ppm (part per million). As an example, a rectangular piece (30×80 mm²) of thickness 3 mm and 5 mm is removed from the front of the pole piece, as shown in Figure 9 and Table 2. If the diameter of ROI is assumed to be 20 mm, then the inhomogeneity value (η) will be less (for example for h=0 mm: $\eta = 356\ ppm$). According to values are given in Table 2 (which are achieved by Excel), it is preferable that the pole piece face connected to PM piece will be flat and free of dentin.
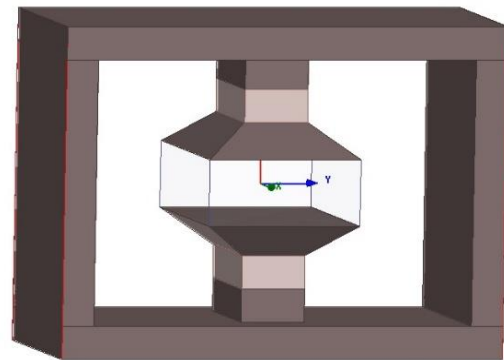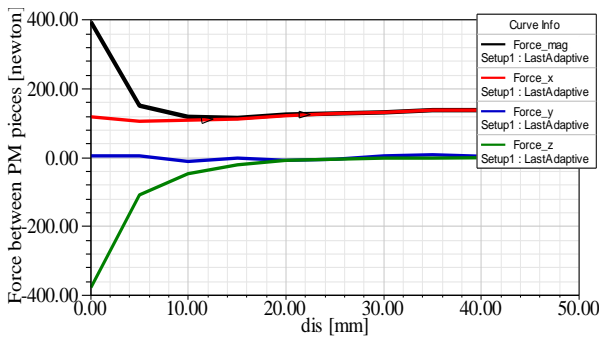

Figure 1. The force between two PM pieces (without pole pieces)

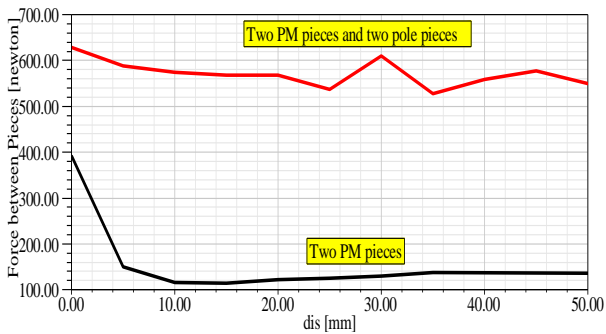**Figure 2.** Comparison between two modes: pole pieces usage and no pole pieces usage
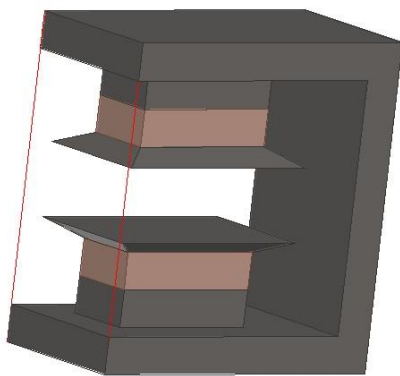

Figure 3. One- side core

Figure 4. Two- side core

TABLE 1. Dimensions of two configurations (with thickness 25 mm)

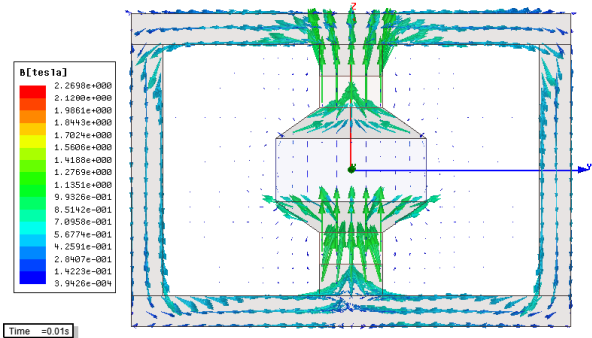| Dimensions	One-sided	Two-sided
Yoke (mm³)	110×210×220	170×250×350
Pole spacers and PM pieces (mm²)	50×100	50×100
Second face of pole pieces (mm²)	90×140	120×170

Figure 5. Distribution and direction of magnetic field density (front view)
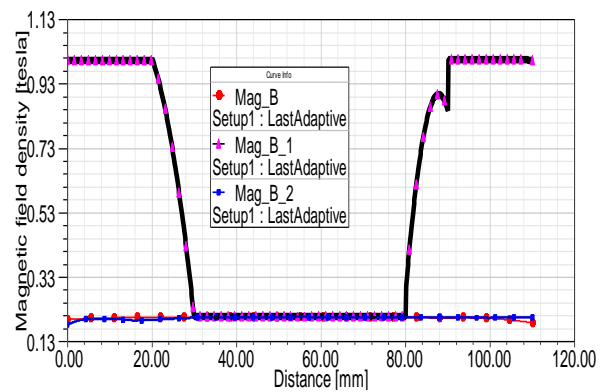

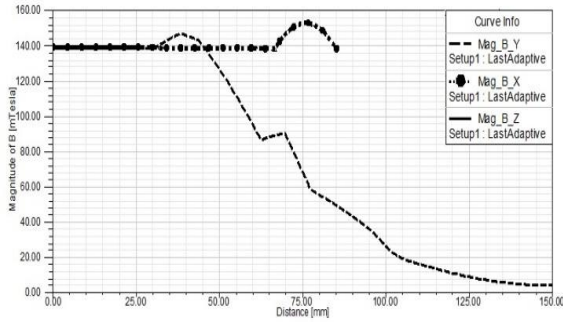**Figure 6.** Magnetic field distribution for the one-sided core

Figure 7. Magnetic field density in x, y and z-axes in the different distances from the core center. Solid, dotted and dashed lines show respectively the distribution of the magnetic field density on the x, y and z-axes
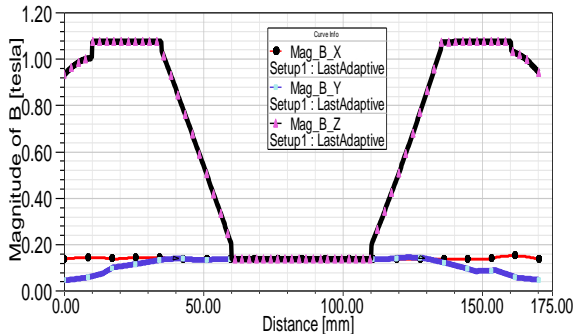

Figure 8. Magnetic field density in equal distances (-85 (mm) to 85 (mm)) for two-sided core. The symbol styles circle, box, and triangle are respectively used for the magnetic field density on the x, y, and z-axes
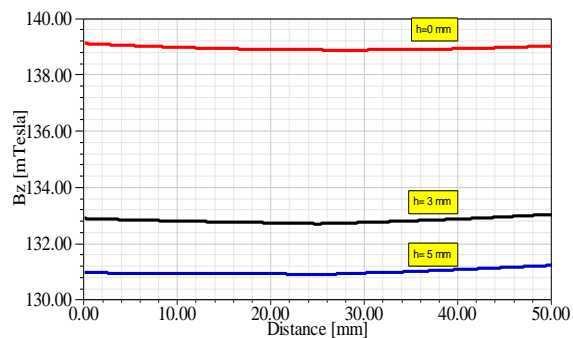

Figure 9. Distribution of magnetic field density for creating a concavity in the face of the pole piece

TABLE 2. The effect of creating the denture at the face of pole piece in the inhomogeneity

Thickness	B_{max}	B_{min}	B_{mean}	η (ppm)
0 mm	139.1	138.88	138.9	1664
3 mm	133.0	132.71	132.8	2499
5 mm	131.2	130.91	131.0	2464

3. 2. Active Shimming As it is shown in Figure 10, by adding small pieces of PM (Smco24) to the greater face of pole pieces, the magnetic field density is increased. It is observed that the magnetic field density in the air-gap centre is about 1.12 times increased but inhomogeneity will not be smaller. There are two ways to solve this problem: (1) use of optimization methods to get the best possible layout of small magnetic pieces with optimized dimensions, (2) use of magnetic tapes at the edges of the pole pieces.

4. IRON CORE CONSTRUCTIONS

After extensive studies, it was decided to build a PM static coil. There should always be an equilibrium point between some design parameters. For example, raising the flux cross-section (product of the thickness and the width of iron pieces) increases the weight and decreases the magnetic field density which is not desirable. The distance between two magnet pieces (the distance between the two PM pieces supported by two iron faces or the length of the non-supporting iron faces or the distance between the pole spacers), and the horizontal and vertical spacing between the iron faces and the PM pieces should be such that the balance of magnetic force will be maintained.

Work routine: First, the thick iron sheet (low carbon steel sheet is used in literature [14]) is placed on a CNC table with a magnetic lifter, and then the cutting direction and size are determined by the user on the monitor. Next, the cutting operation is performed with the flame movement. Now, the cut pieces become very hot. The parts are then transferred to a lathing workshop, on which milling operation is performed to make smooth and uniform side surfaces. This step is a prerequisite for a precise welding. Then, the upper and lower surfaces of the parts are smoothened and polished by magnetic stones. This should be done by the alternator and large industrial clamps because the conventional welding machine is not suitable for thick sheets. A large extent of welding pen was used for this work. At this stage, the
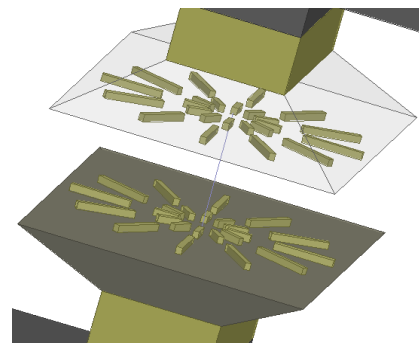

Figure 10. Active shimming by PM pieces. The upper pole piece is shown by 100% transparency.

milling is done again. The result of the work is represented in Figure 11.

Required pieces in which all dimensions are in mm:
1) Two super strong Neodymium magnets N42 100×50×25: thick rare earth NdFeB (Neodymium Iron Boron) block permanent magnets.
2) Two cap polar pieces (are known as slanted pieces) are lathed from two blocks 170×120×25 iron pieces which are displayed in Figure 12.
3) Two blocks 100×50×25 iron pieces known as spacers.
4) Two rectangular 350×170×25 iron sheets.
5) Two rectangular 200×170×25 iron sheets.

4. 1. Installing PM Pieces and Measurement

Initially, the poles of each magnet must be specified. Then, the pole is marked by the letters A and B. Next, two PM pieces should be placed on the smaller face of two slanted pieces. One is installed with pole A and the other with pole B. The pole piece should be tightly held on the ground and the PM is placed on the pole piece by a thin metal sheet (as a handle) and the cork piece; otherwise the PM strikes sharply to the pole piece and breaks (the PM material is extremely fragile). Then, the two piece-pairs are carefully installed on the two spacers by the cork piece with the help of each other. The final air-gap is 4.6 mm. The static coil, which is indicated in Figure 13 (the core is dyed), is now ready for the measurement routine.

Figure 11. Iron core to prevent the dispersion and leakage of magnetic flux (polar spacers are welded to the core yoke)

Figure 12. A slanted piece which is used to simplify the installation of PM parts and to improve the magnetic field
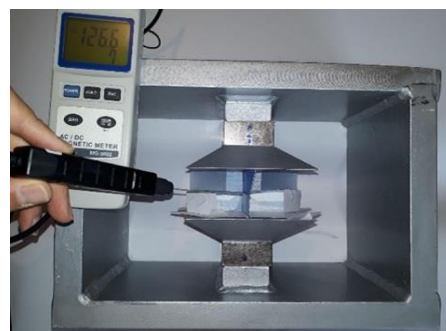

Figure 13. Measuring the static magnetic field density by Lutron MG-3002 (the iron core is painted).

4. 2. Magnetic Field Density Measurement

Method: the measurement can be done in circular or rectangular layers at the surface of PM pieces. The measurement in the air gap is performed at the surface of spherical ROI. Density measurements are made at the intersection of longitudinal (e.g. 12) and transverse arcs (e.g. 13). In the circular area of sampling, the outer circle diameter is 5 cm (because the width of PM is not larger than 5 cm) and diameters are plotted at 15° interval. In addition to determining the location of the measurements, these circles are also used to determine the location of the shimming pieces. Tesla Measurement is done by Lutron (model MG-3002), which is notably affected by the gravity of earth. In the first step, the magnetic field density is measured on a hypothetical plane (parallel to the two pole pieces) at the middle of air distance. This measurement is displayed in Figure 14. The field measurement at the face of two pole pieces is illustrated in Figures 15 and 16. The data related to these figures are given in Tables 3-5. As can be seen, the measured values are not very close. Then, the pole-piece structure requires additional shimming. In the second step, Tesla measurement is done on the surface of spherical volume (diameter=3.8 mm) whose inhomogeneity is 19314 ppm which is large and thus it is best to optimize the design. According to Figures 14-16, the magnetic field density value in the centre of the air-gap is 130 mT, which is adequate for MRI tests.
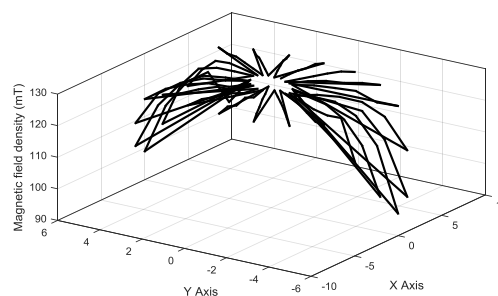

Figure 14. Magnetic field density measurement plane in the middle of the air gap
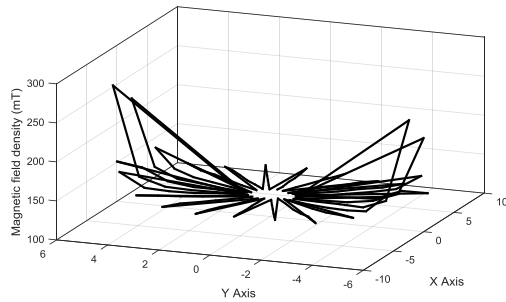
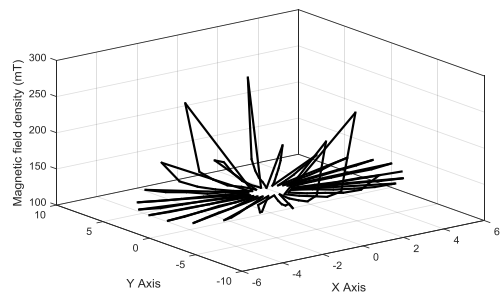**Figure 15.** Magnetic field density measurements on the face of the pole piece A

Figure 16. Magnetic field density measurements on the face of the pole piece B

TABLE 3. The detail data supporting Figure 14

Angle [°]	Distance [cm]					
	1	2	3	4	5	6
0	129.5	129.6	129.5	129	129	128
15	129.6	130	130	130	129	128.5
30	130	130	130	130	129	129
45	130	130	130	130	129	125
60	130	130	130	128.8	124	127
75	130	129.6	129	127	120	106
90	129	120.5	128.5	124	115	99
105	129	129	128.5	125	117	103
120	129.5	129	129	127	123	113
135	129	128	129	128.5	127	123.6
150	129	128	129.4	129	128.1	128
165	128.5	128	128.8	128.5	128.7	127.6
180	128.5	127.5	128.7	127.5	128.5	127.5
195	130	129.4	129.3	128.5	128	127
210	129	129	129	128.8	128	127
225	129	129	129	128	127	128
240	128	128	127	126	128	116
255	128	128.7	128	125	118.5	104
270	128	128	128	125	117	97
285	128	127	126	125	117	100
300	126	127	127	126	122	112
315	129	129	128.3	127.5	124	123
330	129	129.3	129	128	127.6	126.6
345	129	129	129	129	128.8	127.8

TABLE 4. The detail data supporting Figure 15

Angle [°]	Distance [cm]					
	1	2	3	4	5	6
0	129	128	129.3	129	130	132
15	129.1	128.4	129.1	129.3	129.3	132.1
30	129.3	129.1	128.2	129.3	129.8	128.4
45	128	128	129.1	120.4	129.8	133.4
60	125.7	126.8	127.9	129.1	134.6	156.5
75	126.8	127.1	129.1	120.4	141.5	225
90	128	128	128	132	146.5	151
105	126.8	127.4	128.2	130.7	141.7	257
120	128	129	129	131	135	155
135	129	128.8	129.3	130.7	132.7	134.3
150	128	128	128.7	129	130	128.2
165	127	127	127	128	128	127
180	128	128.4	128.8	128.4	129.3	129.6
195	127	126.4	126.8	126.8	128	129.3
210	129	128.4	126.8	127.4	129.6	127
225	128	128	127.7	128.4	131	133
240	126.3	126	127	129	133	157
255	127	128	129	129.3	142	250
270	127.7	127	128	133	145	220
285	128	129	130	130	142	241
300	127.4	126.8	130	132.7	136.8	154
315	127.7	127.7	128.4	130.4	131	134.8
330	127.4	128.8	129.6	129.1	130.7	129.3
345	128.8	129.3	129.6	130.2	130.4	131

TABLE 5. The detail data supporting Figure 16

Angle [°]	Distance [cm]					
	1	2	3	4	5	6
0	130	131	130.9	131.1	130.6	133
15	130.6	131	131.1	131.4	131	132
30	130.6	130.7	129.7	130	131.7	131.9
45	130.4	130	130.1	132	133.1	135.6
60	130.5	129.5	131.5	133.2	137.2	152
75	128.4	130.3	130.2	134	144	251.4
90	130	129	130	136	147	145
105	129	130	129	134	142	234
120	129	128.1	129.1	131.8	138	163
135	130.8	130.7	129	132	133	137.1
150	130.7	130.8	130.7	130.4	130.3	131.1
165	130	130	130	129.4	128.9	131.3
180	130	130.3	129.5	130	130.4	131.8
195	130	128.4	130	129.4	128.9	130
210	130	129.8	128.6	129.8	130	130
225	130	129	129.7	129.6	130.6	134
240	130	130.1	130	129.4	134.8	152
255	130	129.1	129.8	133.7	142	142
270	130	129	131	134	147	226
285	128.6	129.4	131.6	133.6	144	256
300	129	129	130.6	131.7	137	158
315	130.9	130.6	129.3	129.7	131	135
330	129.5	128.7	130.1	130.4	130.2	131
345	130	129.5	128.9	129.8	129.7	130.2

5. CONCLUSION

Through simulation and laboratory work, it was observed that use of rectangular PM piece is possible as the magnitude size and homogeneity of the magnetic field density are desirable. In the first step, the size of the magnet was selected, and then the dimensions of iron core were optimized to achieve the balance of force. In the next step, the iron core was made and the optimized pole piece was lathed to obtain the minimum inhomogeneity. Next, the magnetic field density was measured in the middle of the air gap and on the surface of pole piece by an accurate Tesla-meter and with the help of graded pages because the accuracy of the measurement affects on the RF probe design.

6. REFERENCES

1. Cheng, Y. Y., Xia, L., and He, W., "Simulation and Optimization of a Permanent Magnet for Small-Sized MRI by Genetic Algorithm", *Applied Mechanics and Materials*, Vol. 341–342, (2013), 577–580.

2. Cheng, Y., He, W., Xia, L., Liu, F., "Design of Shimming Rings for Small Permanent MRI Magnet Using Sensitivity-Analysis-Based Particle Swarm Optimization Algorithm", *Journal of Medical and Biological Engineering*, Vol. 35, No. 4, (2015), 448–454.

3. Yao, Y., Koh, C. S., and Xie, D., "Three-Dimensional Optimal Shape Design of Magnetic Pole in Permanent Magnet Assembly for MRI Taking Account of Eddy Currents Due to Gradient Coil Field", *IEEE Transactions on Magnetics*, Vol. 40, No. 2, (2004), 1164–1167.

4. Wang, Q., Wang, H., Zheng, J., Dai, Y., Zhu, X., He, Q., Cheng, J., Chen, S., Song, S., Zhao, B., and Cui, C., "Open MRI Magnet With Iron Rings Correcting the Lorentz Force and Field Quality", *IEEE Transactions on Applied Superconductivity*, Vol. 24, No. 3, (2014), 1–5.

5. Zhu, X., Wang, H., Wang, H., Li, Y. and Fang, Y., "A Novel Design Method of Passive Shimming for 0.7-T Biplanar Superconducting MRI Magnet", *IEEE Transactions on Applied Superconductivity*, Vol. 26, No. 7, (2016), 1–5.

6. Grau-Ruiz, D., Rigla, J.P., Díaz-Caballero, E., Nacev, A., Aguilar, A., Bellido, P., Conde, P., González-Montoro, A., González, A.J., Hernández, L., and Iborra, A., "Feasibility study of a gradient coil for a dedicated and portable single-sided MRI system", In 2016 IEEE Nuclear Science Symposium, Medical Imaging Conference and Room-Temperature Semiconductor Detector Workshop (NSS/MIC/RTSD), IEEE, (2016), 1–4.

7. Peña, A., "B0 Shimming using Pyrolytic Graphite," Master thesis, Leiden University, Netherlands, (2017).

8. Yaghoobpour Tari, S., "Optimization of a Non-axial Magnet Design for a Hybrid Radiation Treatment and MR Imaging System", Doctoral dissertation, University of Alberta, (2017).

9. Noguchi, S., Seungyong Hahn, and Iwasa, Y., "Passive Shimming for Magic-Angle-Spinning NMR", *IEEE Transactions on Applied Superconductivity*, Vol. 24, No. 3, (2014), 1–4.

10. Weggel, C. F. and Weggel, R. J., "New, 'Super-Open,' MRI, and MRT Magnets", *IEEE Transactions on Applied Superconductivity*, Vol. 24, No. 3, (2014), 1–5.

11. Punzo, V., Besio, S., Pittaluga, S., and Trequattrini, A., "MRI Magnet Pole Plate Optimization Method by Fourier Decomposition", *IEEE Transactions on Applied Superconductivity*, Vol. 22, No. 3, (2012), 4401804–4401804.

12. Wu, C., Guo, J., Chen, C., Yan, G., and Li, C., "Optimal Design and Test of Main Magnet in Superconducting MRI", *IEEE Transactions on Applied Superconductivity*, Vol. 20, No. 3, (2010), 1810–1813.

13. Ren, Z., Xie, D., and Li, H., "Study on shimming method for open permanent magnet of MRI", *Progress In Electromagnetics Research M*, Vol. 6, (2009), 23–34.

14. Zimmerman, C.L., "Low-field classroom nuclear magnetic resonance system," Doctoral dissertation, Massachusetts Institute of Technology, (2010).

Static Coil Design Considerations for the Magnetic Resonance Imaging

M. Shiravi[a], B. Ganji[a], A. Shiravi[b]

[a] Department of Electrical & Computer Engineering, University of Kashan, Kashan, Iran
[b] Department of Radiology, Faculty of Medicine, Tehran University of Medical Sciences, Tehran, Iran

چکیده

یکی از چالش‌های اصلی در توسعه سیستم‌های MRI ساخت یک کویل استاتیکی برای تولید چگالی میدان مغناطیسی با ویژگی‌های یکنواختی و اندازه دامنه بهینه می‌باشد. برای این منظور، دو قطعه مکعبی شکل آهنربا از نوع N42 استفاده می شود. در ادامه قطعات آهنی بوسیله CNC تراشکاری می‌شود و قطعات یوغ و ته قطب‌ها جوشکاری می‌گردد. سپس قطعات سرقطب و آهنربا نصب می‌شود. در نهایت، برای ارزیابی عملکرد کویل استاتیکی، میدان مغناطیسی بوسیله تسلامتر Lutron اندازه‌گیری می‌گردد.